

This is an Open Access document downloaded from ORCA, Cardiff University's institutional repository: <https://orca.cardiff.ac.uk/id/eprint/98119/>

This is the author's version of a work that was submitted to / accepted for publication.

Citation for final published version:

Prakash, Muthuramalingam, Lemaire, Thibault, Caruel, Matthieu, Lewerenz, Marius, de Leeuw, Nora H. , Di Tommaso, Devis and Naili, Salah 2017. Anisotropic diffusion of water molecules in hydroxyapatite nanopores. *Physics and Chemistry of Minerals* 44 (7) , pp. 509-519. 10.1007/s00269-017-0878-1

Publishers page: <http://dx.doi.org/10.1007/s00269-017-0878-1>

Please note:

Changes made as a result of publishing processes such as copy-editing, formatting and page numbers may not be reflected in this version. For the definitive version of this publication, please refer to the published source. You are advised to consult the publisher's version if you wish to cite this paper.

This version is being made available in accordance with publisher policies. See <http://orca.cf.ac.uk/policies.html> for usage policies. Copyright and moral rights for publications made available in ORCA are retained by the copyright holders.



Anisotropic diffusion of water molecules in hydroxyapatite nanopores

Muthuramalingam Prakash¹ · Thibault Lemaire¹ · Matthieu Caruel¹ ·
Marius Lewerenz³ · Nora H. de Leeuw² · Devis Di Tommaso⁴ · Salah Naili¹

Abstract New insights into the dynamical properties of water in hydroxyapatite (HAP) nanopores, a model system for the fluid flow within nanosize spaces inside the collagen-apatite structure of bone, were obtained from molecular dynamics simulations of liquid water confined between two parallel HAP surfaces of different sizes ($20 \text{ \AA} \leq H \leq 240 \text{ \AA}$). Calculations were conducted using a core-shell interatomic potential for HAP together with the extended simple point charge model for water. This force field gives an activation energy for water diffusion within HAP nanopores that is in excellent agreement with available experimental data. The dynamical properties of water within the HAP nanopores were quantified in terms of the second-order water diffusion tensor. Results indicate that water diffuses anisotropically within the HAP nanopores, with the solvent molecules moving parallel to the surface

twice as fast as the perpendicular direction. This unusual dynamic behaviour is linked to the strong polarizing effect of calcium ions, and the synergic interactions between the water molecules in the first hydration layer of HAP with the calcium, hydroxyl, and phosphate ions, which facilitates the flow of water molecules in the directions parallel to the HAP surface.

Keywords Hydroxyapatite · Water confinement · Molecular dynamics · Hydrogen bonding · Anisotropic diffusion

Introduction

The macroscopic properties of bone tissue are tightly coupled to molecular processes taking place at the interface between Hydroxyapatite minerals (HAP, molecular unit formula $[\text{Ca}_{10}(\text{PO}_4)_6(\text{OH})_2]$) and water within the lacuno-canalicular network (Sansalone et al. 2013). In particular, the formulation of theoretical models for the prediction of tissue behaviour under the influence of time-dependent external stress inducing internal remodelling requires a detailed understanding of the dynamics of water and its interaction with the surface of HAP surfaces. Mechanics modelling to describe the mechanical behaviour of bone at the macroscopic scale are based on homogenization and micromechanical methods which are powerful tools not only to obtain the overall behaviour of the material via the determination of the overall properties, but also to obtain information about the microfields which are defined at the microscale and are associated with the local distribution of the macrofields. Macroscopic predictions of either part or all of the elastic modulus tensor have been given by many authors (Yoon

*\ Devis Di Tommaso
\ d.ditommaso@qmul.ac.uk

*\ Salah Naili
\ salah.naili@univ-paris-est.fr

¹\ Laboratoire Modélisation et Simulation Multi Echelle,
MSME UMR 8208 CNRS, Université Paris-Est,
Créteil Cedex 94010, France

²\ School of Chemistry, Cardiff University, Main Building, Park
Place, Cardiff CF10 3AT, UK

³\ Laboratoire Modélisation et Simulation Multi Echelle,
MSME UMR 8208 CNRS, Université Paris-Est,
77454 Marne la Vallée Cedex 2, France

⁴\ School of Biological and Chemical Sciences, Queen Mary
University of London, Mile End Road, London E1 4NS, UK

and Cowin 2008; Sansalone et al. 2012 ; Hellmich and Katti 2015). In this context, bones with different forms of water will display differences in stiffness and strength.

HAP scaffolds constitute a prototypical model of bio-material-based surfaces (Kandori et al. 2000b; Rimola et al. 2012; Corno et al. 2010) and have been used in several studies of bone repair (Oddou et al. 2011). These substitutions HAP-based materials allowed the investigation of the interactions between HAP surfaces with biomolecules (Almora-Barrios et al. 2009; Katti et al. 2010; Kandori et al. 2000a; Hernandez et al. 2015; Lukasheva and Tolmachev 2015), water (Zhao et al. 2014), ions (de Leeuw 2004a , b; Sakhno et al. 2010), and gases (Chi-atti et al. 2013). Water plays a crucial role during bone mineralization and in the protein interaction (Corno et al. 2010; Qin et al. 2012; Nair et al. 2014; Lemaire et al. 2015a) as they can act as a prominent charge carrier, transporting ions (Prakash et al. 2009; Prakash and Subramanian 2011) and maintaining the pH of the medium. When considering cells nanopores of transmembrane proteins (Hille 2001) or bone nanopores (Pham et al. 2015), the interactions between water molecules and the polar groups of HAP (calcium (Ca^{2+}), phosphate (PO_4^{3-}), and hydroxyl (OH^-) ions) may affect the local environment of the interface, modifying the diffusion of water molecules, which tend to be reduced when compared with the bulk (Bhide and Berkowitz 2005; von Hansen et al. 2013; Lemaire et al. 2015b).

The unusual dynamics of water and other molecules under confinement has been subject to several experimental and theoretical studies (Tan et al. 2005; Sendner et al. 2009; Su and Guo 2011; Nguyen and Bhatia 2012; Bourg and Steefel 2012; Srivastava et al. 2012; Xu et al. 2013; Planchais et al. 2014; Prakash et al. 2015; Han et al. 2015; Qiu and Huang 2015; Nie et al. 2016). In particular, nuclear magnetic resonance (NMR) techniques showed that water diffuses anisotropically inside nanoporous systems (Cleveland et al. 1976; Thomsen et al. 1987; Wei et al. 2011; Salles et al. 2011) and two different self-diffusion coefficients of water were measured in sheep Achilles tendon using pulsed-field-gradient stimulated-echo NMR (Fechete et al. 2005). However, the molecular-level details regarding the diffusion mechanism of water molecules in the vicinity of the HAP bone surface, the origin of this anisotropic diffusion behaviour, and the interactions at the interface responsible for the preferential movement of water molecules towards a particular direction, remain unclear.

Owing to advances in theoretical models and techniques, atomistic simulation methods are particularly suited to obtain a molecular-level characterization of the solid-water interface (Kirkpatrick et al. 2005; Kubicki 2016), including a direct exploration of the structure and dynamics of water in contact with a mineral (Parvaneh et al. 2016).

In this study, we present classical molecular dynamics (MD) simulations of liquid water in hydroxyapatite nanopores of different pore sizes. The aim of this work is to investigate the dynamical properties of water, and changes therein with varying pore sizes. In particular, the concept of self-diffusion tensor originally introduced by Kubo (1957) has been applied to compute all nine Cartesian components of the three-dimensional diffusion. As the diffusion coefficient is a scalar quantity and cannot, therefore, quantify the preferential movement of water molecules in a particular direction, in this work, we computed the anisotropic diffusion of water within HAP nanopores in order to determine the effect of confinement on its dynamic behaviour.

Theoretical models and methods

HAP surface and water models

Hydroxyapatite (HAP given by $\text{Ca}_{10}(\text{PO}_4)_6(\text{OH})_2$) is viewed as an hexagonal primitive cell with $P6_3/m$ space group. The nanopore is represented by a face-to-face configuration of parallel HAP platelets. Its size corresponds to the narrowest pore diameters measured in bones by Holmes et al. (1964). This geometrical configuration is motivated by the fact that, in bone tissue, hydroxyapatite is present in the form of thin micro-plates with dimensions ($L \times \times e$), where $L = 250\text{--}500 \text{ \AA}$ (in 1-direction), $= 150\text{--}250 \text{ \AA}$ (in 2-direction) and $e = 25 \text{ \AA}$ (in 3-direction) (Weiner and Traub 1986). Cell parameters and crystallographic data of Sudarsanan and Young (1969) were used for the initial configuration of the HAP structure. The dimensions of the parallelepiped-shaped simulation box were adjusted to contain $3 \times 3 \times 4$ such micro-plates. The position of each atom in the box is given using the vector position whose the cartesian coordinates are denoted by (r_1, r_2, r_3) in the orthogonal frame (1, 2, 3) (see Fig. 1).

The HAP platelets and water layers constituted the elementary unit cell for our simulations. HAP nanopores were generated by varying the c -axis of the crystal from $H = 20 \text{ \AA}$ to $H = 240 \text{ \AA}$. The resulting surface corresponds to the (0001) basal plane, which is the dominant surface in the thermodynamically-stable morphology (Mkhonto and de Leeuw 2002) and is important in biological systems, as the elongation of the bone platelets along the c -direction of the apatite crystal results in the expression of this surface (Rohanizadeh et al. 1999). In addition, experimental evidence shows that these faces act as the binding site for many adsorbates (Wierzbicki and Cheung 2000).

For all pore sizes, the atomic configuration editor Aten (Young 2016) was used to fill the resulting vacuum with water molecules corresponding to the experimental density of 1 g cm^{-3} .

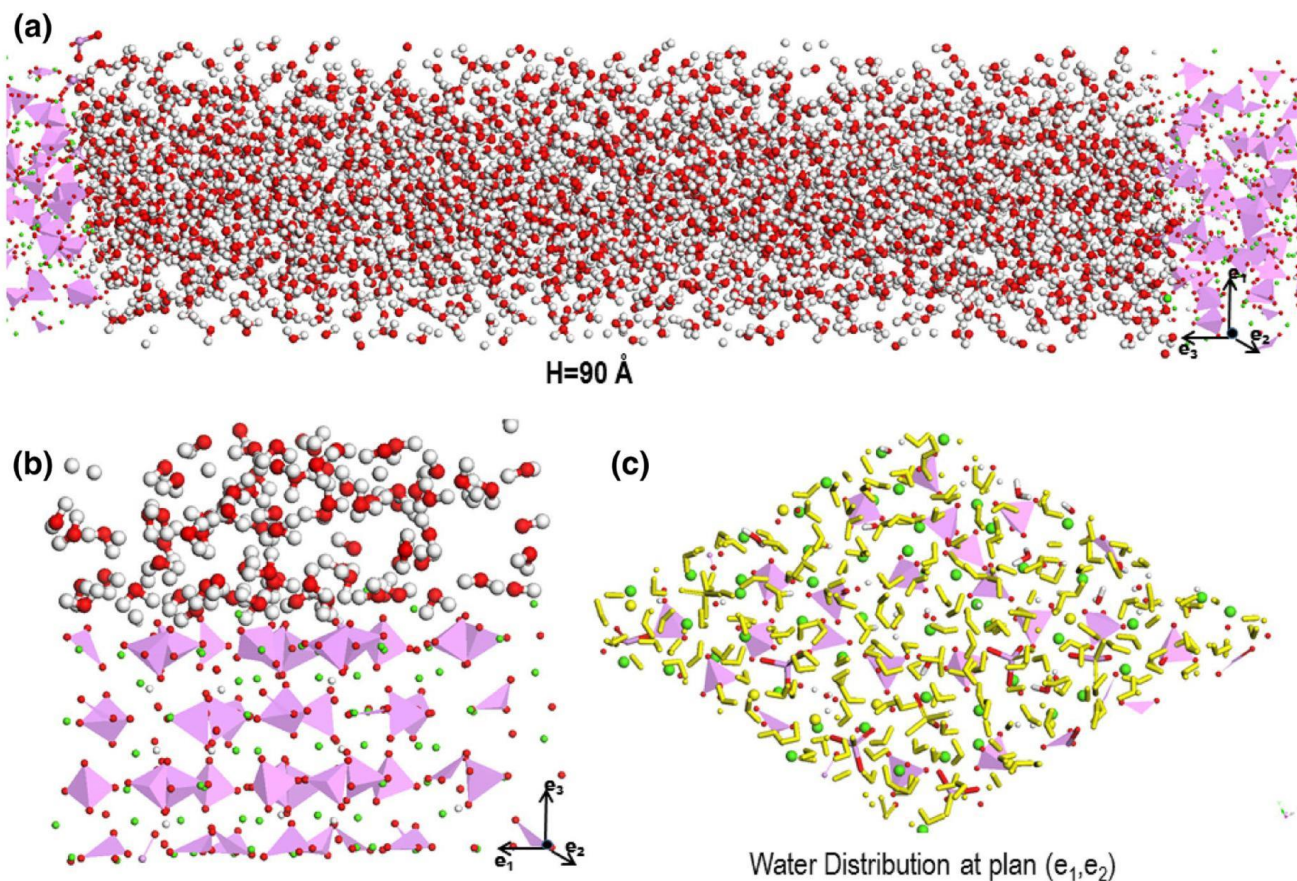


Fig. 1 HAP-water system (Ca-green, PO_4^{3-} -pink, O-red, and H-white) with a pore size of 90 Å. **a** Unit cell of the HAP nanopore—water used in the simulations. **b** Side view of the HAP-water interface. **c** Top view of the HAP-water interface

Molecular dynamics

All MD simulations were performed using the DL_POLY 4.05.1 code (Todorov et al. 2006). Interatomic potentials for HAP and its interaction with water are the ones developed by de Leeuw (2004a) and de Leeuw and Parker (1998). The water molecules were represented using the extended simple point charge (SPC/E) potential (Berendsen et al. 1981). The potential parameters used in this work are reported in electronic supporting material (see Tab. S1).

Each system considered in the present study was first equilibrated for 50 ps in the microcanonical (NVE) ensemble. This was followed by an equilibration period in the isothermal–isobaric (NPT) ensemble ($P = 1 \text{ atm.}$ and $T = 300 \text{ K}$) during which the volume was monitored to confirm the system reached equilibrium. The behaviour of the volume for the nanopores with $H = 20, 60$ and 110 \AA is reported in Fig. S2 of electronic supporting information. This was followed by 2 ns of production period in the NPT ensemble. All simulations used the Nosé–Hoover algorithm with 0.5 and 0.5 ps as the thermostat and barostat relaxation times, respectively. To mimic the in vivo human bone

environment, simulations were performed at temperature of 310 K unless otherwise stated. The Verlet leapfrog scheme with a time step of 0.1 fs was used to integrate the equations of motion. Periodic boundary conditions were applied in all three directions of the unit cell. The long range electrostatic interactions between the charges of all species were computed using the Smoothed Particle Mesh Ewald (SPME) method with a relative error of 10^{-6} (Essmann et al. 1995). Table 1 lists the number of atoms in HAP (N_{HAP}), which included core-shell atoms, number of water molecules NO , duration of each simulation T_D , and initial H and equilibrated H^* values of the pore sizes. Notice that the equilibrium height of the pore size is close to the initial one, which justifies the use of the NPT ensemble instead of NVT for our simulations. The structure of the HAP nanopore–water systems considered in the present study is reported in Tab. S3 of electronic supporting material.

To verify if HAP nanopores and the surface retained the crystalline structure, we computed the phosphorous–phosphorous (P–P) radial distribution functions (RDFs) of the hydroxyapatite crystal, and of the bulk and surface of the HAP ($H = 110 \text{ \AA}$) nanopore in contact with water (see

Table 1 Details of the molecular dynamics simulations of the HAP nanopores-water systems: number of atoms in HAP N_{HAP} , number of water molecules N_{O_w} , duration of each simulation T_{D} (in ns), initial H (in Å), and equilibrated H^* (in Å) pore sizes

H (in Å)	N_{HAP}	$N_{\text{H}_2\text{O}}$	T_{D} (in ns)	H^* (in Å)
20	2520	455	2	21.6
30	2520	682	2	32.8
40	2520	910	2	41.3
50	2520	1138	2	52.7
60	2520	1363	2	64.1
70	2520	1593	2	71.4
80	2520	1820	2	82.7
90	2520	2048	2	92.4
100	2520	2276	2	103.9
110	2520	2506	2	112.6
120	2520	2732	2	124.6
130	2520	2960	2	135.3
160	2520	3650	1	167.3
200	2520	4550	1	196.8
240	2520	5300	1	228.1

Fig. S4 of electronic supporting material). The P–P RDF profile of the nanopore is very similar to that of the crystal, which indicates that HAP nanopores remain crystalline. The P–P RDF profile of the HAP surface shows some deviations compared with that of HAP nanopore, suggesting some restructuring of the surface but not to an extent to indicate amorphousization of the surface (Tian et al. 2016). This agrees with the previous MD work by de Leeuw, which showed that HAP surfaces maintain its crystalline structure (de Leeuw 2004a, b).

Validation of the theoretical methodology

We have used the SPC/E water model, because it gives a density, radial distribution functions, and self-diffusion coefficient for water in good agreement with experiment (Berendsen et al. 1987). In particular, the value of self-diffusion coefficient D_{S} for bulk SPC/E water obtained from a molecular dynamics simulation of 729 water molecules (NPT ensemble, 2 ns of production period) is $2.58 \times 10^{-9} \text{ m}^2/\text{s}$, in good agreement with the experimental value of $2.999 \times 10^{-9} \text{ m}^2/\text{s}$ (Holz et al. 2000). Moreover, comprehensive calculations of the activation energy of diffusion E_{A} of water in bulk liquid water also concluded that using the SPC/E model, the value of E_{A} is 14.8 kJ/mol, which is only 2.6 kJ/mol lower than the experimental value $E_{\text{A}} = 17.4 \text{ kJ/mol}$ (Holmboe and Bourg 2014). To validate the combination of force fields, molecular models, and computational techniques used in the present work, we compared the activation energy denoted E_{A} for the diffusion of water within HAP nanopores with the experimental values measured for

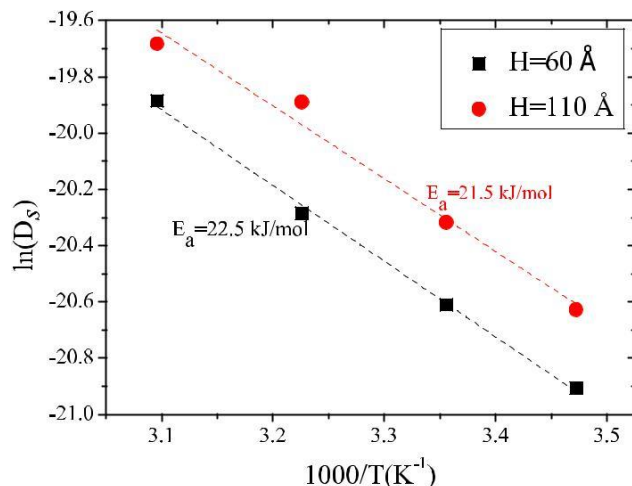


Fig. 2 Arrhenius plots of the average diffusion coefficient of water versus the inverse of the temperature for the HAP-water systems with pore sizes equal to 60 and 110 Å, where H is the initial height of the nanopore

cortical bone and inter-tubular dentine (Fernández-Seara et al. 2002). MD simulations were conducted at the temperatures of 288, 298, 310, and 323 K to determine the activation energy for water diffusion in HAP nanopores with $H = 60 \text{ \AA}$ and $H = 110 \text{ \AA}$ (see Fig. 2), which are representative of typical nanopores in bones ($50 < H < 125 \text{ \AA}$) (Holmes et al. 1964). The activation energies were obtained from the linear fit of the points in Fig. 2 using Arrhenius equation $\ln(D_{\text{S}}) = \ln(D_0) - E_{\text{A}}/(RT)$, and the values of E_{A} are $22.5 \pm 0.7 \text{ kJ/mol}$ for $H = 60 \text{ \AA}$ and $21.5 \pm 2.0 \text{ kJ/mol}$ for $H = 110 \text{ \AA}$, which are very close to NMR measurements in cortical bone ($E_{\text{A}} = 26.6 \text{ kJ/mol}$) and inter-tubular dentine $E_{\text{A}} = 29.5 \text{ kJ/mol}$ (Fernández-Seara et al. 2002). This result validates the molecular models and interaction potentials used in the present work to represent fluid flow within bone sub-micrometer pores. A related point to consider is that the activation energies for water diffusion within the HAP nanopores are higher than in bulk $E_{\text{A}} = 17.4 \text{ kJ/mol}$ (Holmboe and Bourg 2014), which suggests that diffusion of water is hindered by the interaction between water molecules and the polar groups at the HAP surface.

Results and discussion

Self-diffusion coefficient

The self-diffusion coefficient of water, denoted by D_{S} , is a key property when studying the flow of fluid. From an MD simulation diffusion coefficients can be calculated using Einstein relation:

$$D_S = \frac{1}{d_S} \frac{1}{2} \frac{d \langle [r(t) - r(0)]^2 \rangle}{dt} \quad (1)$$

where d_S is the dimension of the space (in this paper $d_S = 3$), $r(0)$ and $r(t)$ are the position vectors at times $t = 0$ and t , respectively, and the angled brackets $\langle \cdot \rangle$ indicate the average over the number of times origin spanned by t and the number of water molecules. However, this scalar quantity cannot describe the differential diffusion of water in directions parallel or perpendicular to the HAP surface (see Fig. 1).

To quantify the anisotropic diffusion of water in the HAP nanopores, we introduce the second-order water self-diffusion tensor D_{ij} , which is defined as follows:

$$D_{ij} = \begin{pmatrix} D_{11} & D_{12} & D_{13} \\ D_{12} & D_{22} & D_{23} \\ D_{13} & D_{23} & D_{33} \end{pmatrix} \quad (2)$$

whose components D_{ij} represent the anisotropic diffusion coefficients and are computed using the following expression which was derived from Kubo (1957):

$$D_{ij} = \frac{1}{2} \frac{d \langle [r_i(t) - r_i(0)]^2 + [r_j(t) - r_j(0)]^2 \rangle}{dt}, \quad i, j = 1, 2, 3. \quad (3)$$

In Eq. (3), $r_i(0)$ and $r_i(t)$ are the components of the position vectors along the i -direction ($i, j = 1, 2, 3$) of the Cartesian frame shown in Fig. 1. The anisotropic diffusion coefficients D_{ij} were computed by modifying the DL-POLY

code. This new utility accurately determines the anisotropic self-diffusion coefficients by computing the mean square displacement (MSD) for the different atomic species in the simulation using multiple time origins as defined by Eq. 3. The mean square displacements associated with the diagonal elements of the anisotropic self-diffusion tensor D_{ij} for $i = 1, 2, 3$ are plotted in the Fig. 3.

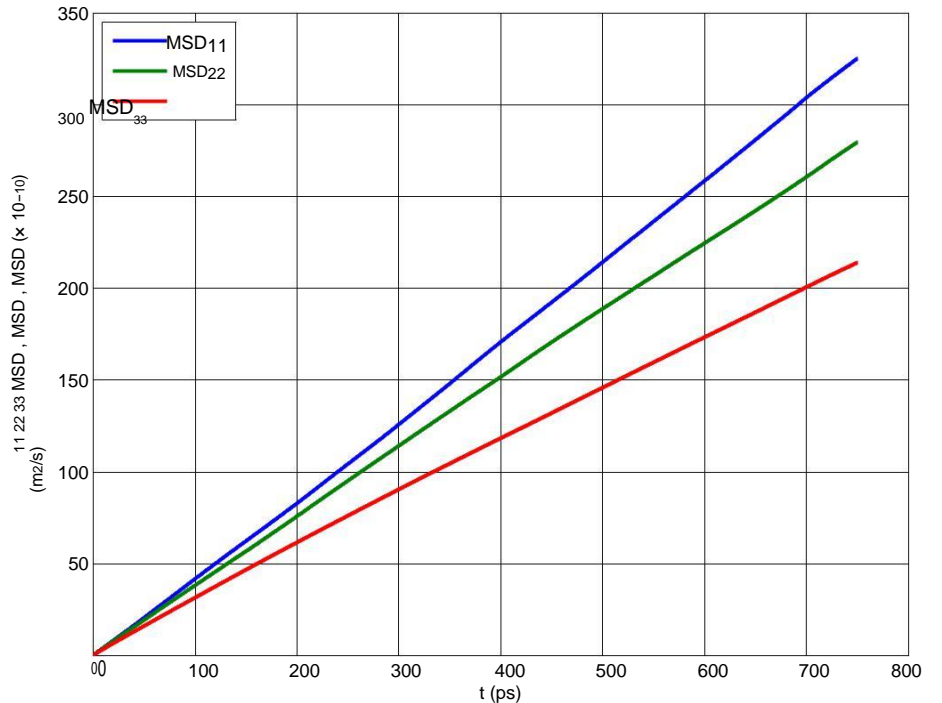
Without attempting an exhaustive list on a subject beyond the scope of this paper, Cummings et al. (1991) have presented different methods for calculating certain self-diffusion coefficients in a non-Newtonian fluid subject to a couette strain field. Furthermore, Liu et al. (2004) have introduced a Einstein–Smoluchowski-like method for calculating the parallel and perpendicular components of the self-diffusion to a surface. Bořan et al. (2011) have used this previous method for studying the self-diffusion in clay nanopores.

The anisotropic diffusion tensor can be decomposed into its so-called spherical and deviatoric parts:

$$D_{ij} = \frac{1}{3} (\text{TRA } D_{ij}) + \text{DEV } D_{ij}, \quad (4)$$

where TRA is trace operator that gives the sum of the diagonal elements of D_{ij} , and the deviatoric part is given by $\text{DEV } D_{ij} = D_{ij} - (1/3)(\text{TRA } D_{ij})$. Any tensor of the form $\lambda \delta_{ij}$, where λ is a scalar, is known as a spherical tensor, while $\text{DEV } D_{ij}$ is known as a deviatoric tensor. Note that an important property of the deviatoric tensors is $\text{TRA } (\text{DEV } D_{ij}) = 0$. This decomposition decouples the “volumetric” from the “distortional” properties

Fig. 3 Mean square displacements associated with the three interest quantities describing the diffusion coefficients D_{ij} for $i = 1, 2, 3$ for $H = 90 \text{ \AA}$



which can be interpreted as a decoupling of the “mean” part from the “fluctuation” part because of the underlying orthogonality of the spherical and deviatoric partitions

$\text{TRA} (\mathbf{S} \times \text{DEV}) = 0$, where $\mathbf{S} = (\mathbf{1}/3)\text{TRA}$. This decomposition mimics the ones of the vectors that can be decomposed uniquely as a sum of two vectors, one tangent to a surface, called the tangential component of the vector, and another one perpendicular to the surface, called the normal component of the vector. As a result, due to the geometry of the HAP nanopores, the matrix representation of the self-diffusion tensor should be diagonal. This was first confirmed by the quasi-nullity of the off-diagonal elements, and then by computing the spherical part of in Eq. (4), which does, indeed, correspond to the standard diffusion coefficient of water calculated using Eq. (1).

The anisotropic diffusion coefficients of water as a function of the pore size are reported in Fig. 4. Our calculations show that the transport properties of water depend significantly on the size of the HAP nanopore (Pham et al. 2015), but also quantify the marked anisotropic behaviour of liquid water when confined within nanosize volumes.

In Fig. 4, for small-to-medium nanopores ($20 \text{ \AA} < H < 70 \text{ \AA}$), the coefficients D_{11} and D_{22} associated with the diffusion along the 1 and 2 directions correspond to the movement of particles parallel to the HAP surface (see Fig. 1), and their values are similar to the isotropic self-diffusion coefficient D_S . For nanopores larger than $>70 \text{ \AA}$, D_{11} is about 15% higher than D_S , whereas $D_{22} \sim D_S$. On the other hand, for all nanopores, the coefficients D_{33} , which correspond to the normal direction to the HAP surface, are significantly lower than both the isotropic coefficient D_S , and the coefficients D_{11} and D_{22} associated with the diffusion parallel to the HAP surface. For example, in the HAP

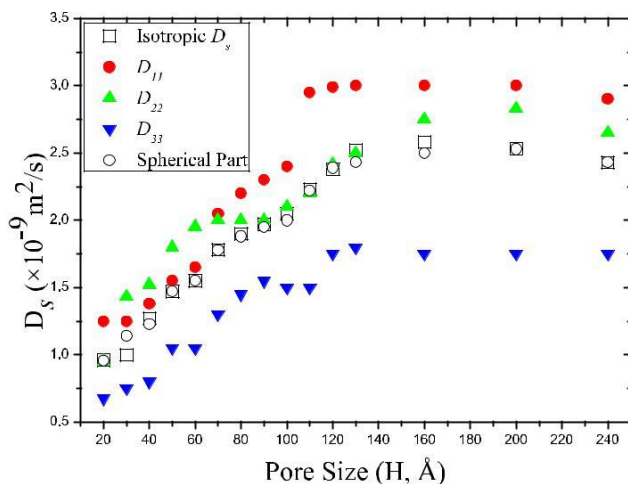


Fig. 4 Anisotropic diffusion coefficients D_{ii} ($i = 1, 2, 3$), standard isotropic diffusion coefficient D_S , and spherical part of the diffusion tensor of water molecules within the HAP nanopores

nanopore with $H = 110 \text{ \AA}$, $D_{33} = 1.5 \times 10^{-9} \text{ m}^2/\text{s}$, and D_{11} and D_{22} are equal to 3.0×10^{-9} and $2.2 \times 10^{-9} \text{ m}^2/\text{s}$, respectively. This signifies that water molecules preferentially diffuse along the HAP surfaces rather than towards the bulk of the aqueous solution in contact with the nanopore. In Fig. 4, the spherical part of the diffusion tensor corresponds to the standard isotropic diffusion coefficient.

This in-plane confinement effect is visually represented in Fig. 5 by the trajectory of a water molecules that is part of the first hydration layer of the HAP nanopore with $H = 110 \text{ \AA}$. A water molecule was considered to be part of the first hydration layer of HAP if the distance between the calcium atoms (Ca) at the HAP surface and the oxygen atoms (O_W) of the water molecules is less than 3.0 \AA . This distance corresponds to the position of the first minimum in the $\text{Ca}^{2+} - O_W$ pair distribution function (e.g., Di Tommaso et al. 2014) as well as the position of the minimum in the number density profile of the oxygen atoms that are closer to the HAP surface. Figure 5 shows that during the dynamics, the tagged water molecule moves approximately parallel to the surface of HAP. A similar conclusion was obtained from the visualization of the trajectories of water molecules that were part of the second hydration layer of HAP. Moreover, the analysis of the motion of the tracer molecule from its initial ($t = 0 \text{ ns}$) to its final ($t = 2 \text{ ns}$) MD

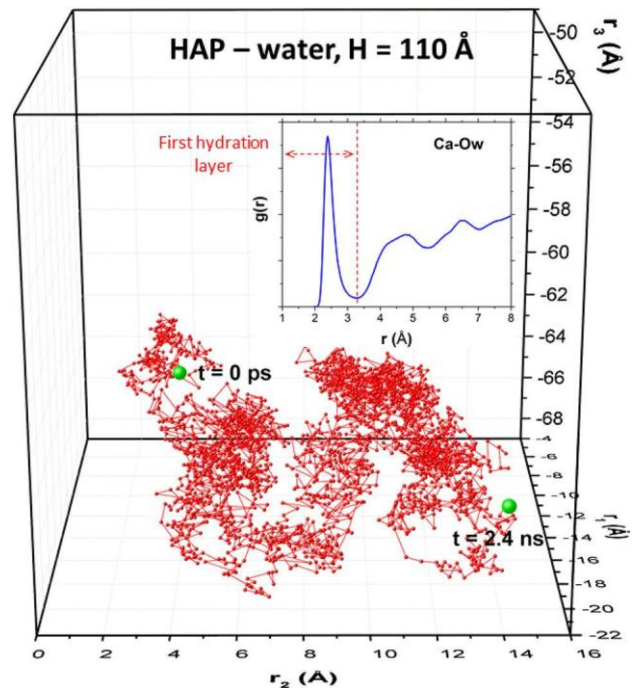


Fig. 5 Motion of a randomly chosen tracer molecule that is part of the first hydration layer of the HAP nanopore with $H = 110 \text{ \AA}$. The inset reports the radial distribution function $[g(r)]$ of calcium ions at the surface and oxygen water atoms (Ca- O_W)

steps indicates that the 1 and 2 components of the position vector change by twice as much as the 3 component. This agrees with the values of the anisotropic diffusion coefficients D_{11} and D_{22} being larger than D_{33} (see Fig. 4). The polarization effect of the calcium ions at the HAP surface, which can extend up to four layers of water (Bolis et al. 2012), can be used to rationalize the slow diffusion of water along the 3-direction observed in our MD simulations.

The time-dependent MSD of the oxygen atoms of water molecules (O_W) close to the HAP-water interface, and further away from it, was also computed using the following expression:

$$\langle \overline{|\mathbf{r}_{O_W,n}(t) - \mathbf{r}_{O_W,n}(0)|^2} \rangle$$

where $\mathbf{r}_{O_W,n}(0)$ and $\mathbf{r}_{O_W,n}(t)$ are the position vectors at times $t = 0$ and t , respectively, and the angled brackets $\langle \cdot \rangle$ indicate the average over the number of times origin spanned by t and the number of water molecules. The subscript $O_{W,n}$ denotes the oxygen atoms that are part of the n -th “layer” of water in the HAP nanopore. For example, a water molecule was considered to be part of the first hydration layer if $d(\text{CA}^{2+} - O_W) < 3.0 \text{ \AA}$. The (water) oxygen atoms used to compute the MSD of a specific hydration layer were determined from the configuration of the first MD step of the production period, and by selecting those O_W atoms such that $d(\text{CA}^{2+} - O_W)$ was within a specific threshold. The MSD of O_W in the hydroxyapatite nanopores with $H = 60$ and 110 \AA for the hydration layers defined by $d(\text{CA}^{2+} - O_W)$ equal to 6 \AA (first and second layer), 20 , 30 , and 40 \AA are reported in Fig. S5 of electronic supporting material. The results indicate that as we move further away from the interface, water molecules diffuse more slowly and this effect becomes more pronounced with the size of the nanopore. However, it is important to notice that several water exchanges were counted between the different hydration layers during the MD trajectories, and consequently, the MSD in Fig. S4 cannot be unambiguously associated to a specific hydration layer of the HAP nanopore.

Hydrogen bonding at the HAP-water interface

Hydrogen-bonding (H-bonding) interactions play a vital role in the movement of water molecules on the HAP surface. Figure 6 shows the molecular arrangement of water molecules on the HAP surface. In particular, Fig. 6a gives a closer view of the orientation of water molecules on the surface and the H-bonded interaction with hydroxyl and phosphate groups of HAP. Visualization of the trajectories revealed a peculiar “rolling” motion for the water molecules. This is illustrated in Fig. 6b–e, where the molecular arrangement of a selected water molecule at four MD steps shows that the H-bonding interactions with the HAP

surface influence the translation and rotation motions of water and facilitate the anisotropic diffusion of water. Figure 7 reports a schematic representation of the rolling motion of water, which occurs via H-bonding interactions, determining a preferential diffusion of water molecules on the (1, 2)-plane.

The H-bonding structure greatly influences the dynamical properties of water (Chandra 2002). The effect of confinement on the distribution of the number of H-bonds was, quantified by scanning the MD trajectories of bulk water and water within HAP nanopores in order to determine the existence of an H-bond between two water molecules based on the following geometrical criteria: (1) the donor–acceptor inter-oxygen distance is less than 3.5 \AA ; (2) the donor–acceptor inter hydrogen-oxygen distance is less than 2.45 \AA ; (3) the hydrogen-donor–acceptor angle is less than 30° (Chandra 2000).

The average number of H-bonds n_{HB} is about 3.5 in bulk liquid water and in the HAP nanopore with $H = 110 \text{ \AA}$, but n_{HB} decreases to 3.4 for $H = 60 \text{ \AA}$, 3.3 for $H = 40 \text{ \AA}$ and 3.0 for $H = 20 \text{ \AA}$, that is, as the degree of confinement increases. This is linked with the increasing influence of the HAP surface on H-bonding network. In fact, the distribution of the number of H-bonds between water molecules coordinated to the HAP surface and the surrounding water molecules (see Table 2) shows that, in liquid water, the majority of water molecules (51%) have a local tetrahedral network, whereas in the first hydration layer of HAP, more than 60% of water molecules have two, one, or zero H-bonds (HBs). In an aqueous environment, the motion of water molecules occurs via the breaking and reforming of H-bonds and the reduction in water diffusion within HAP nanopores can be explained in terms of the lack of water–water H-bonds through which a water molecule can diffuse from the surface to the bulk. Given that water molecules coordinated to the surface form, on average, less than two HBs per molecule with the surrounding water molecules, this implies that they interact with the hydroxyl group and diffuse preferentially along the surface rather than towards the bulk solution.

Conclusion

We conducted classical molecular dynamics simulations of liquid water within hydroxyapatite nanopores of different sizes ($20 \text{ \AA} \leq H \leq 240 \text{ \AA}$) to determine the effect of confinement on the dynamical properties of water. We showed that our core-shell potential for hydroxyapatite together with the standard SPC/E water model gives an activation energy for water diffusion have a local tetrahedral network that is in very good agreement with available experimental data. We identified an anisotropic diffusive behaviour

Fig. 6 Molecular arrangement of water molecules on the HAP surface with $H = 70 \text{ \AA}$ (Ca-green, P-pink, O-red, H-white, and hydroxyl O in blue): **a** H-bonding between hydroxyl ion (HAP) and water molecules: **b-e** motion of selected water molecule (in yellow color circle) on the HAP surface at selected times (in ps)

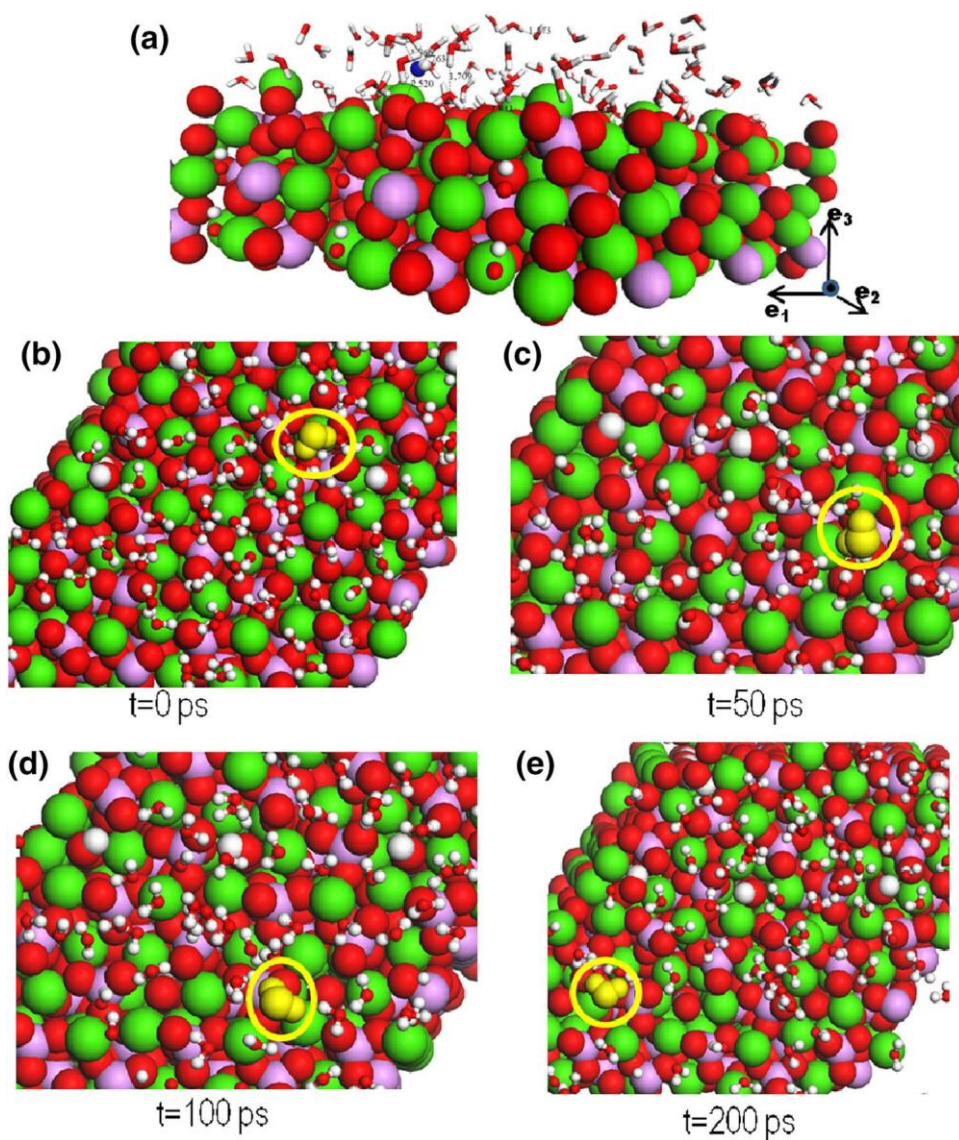


Fig. 7 Schematic representation of the HAP-water interface showing the water adsorption sites and the mechanism of water rolling motion on the HAP surface

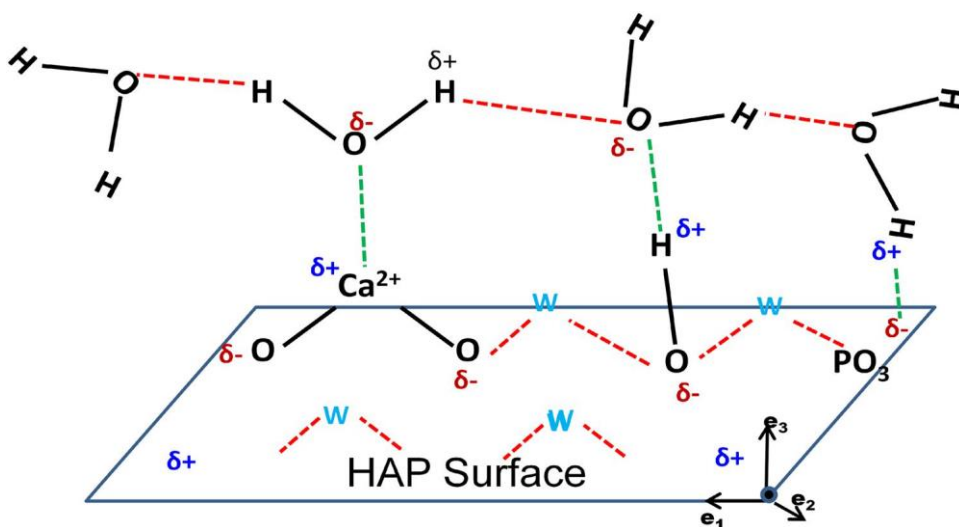


Table 2 Distribution of the number of hydrogen bonds for the water molecules coordinated to the calcium surfaces

	0	1	2	3	4	5	Average
Bulk water	0.0	0.9	0.8	33.0	51.3	5.9	3.53
HAP-water							
110 Å	22.3	22.4	22.0	19.7	12.5	1.0	1.81
60 Å	22.7	22.5	22.0	19.4	12.3	1.0	1.79
40 Å	24.5	23.6	21.4	18.3	11.2	1.0	1.71
20 Å	26.8	27.9	21.2	15.0	8.3	0.7	1.52

Results obtained from molecular dynamics simulations of bulk water and water within HAP nanopores of different sizes ($20 \text{ \AA} \leq H \leq 110 \text{ \AA}$). The values given are percentages of molecules with the given number of hydrogen bonds and the average number of hydrogen bonds per water molecule

for the molecules, which was quantified by defining a self-diffusion tensor, D_{ij} ($i, j = 1, 2, 3$). As a result of the strong interactions between water molecules and the functional groups of HAP, which become dominant in such confined environments, the motion of water molecules in the direction parallel to the surface is significantly faster than in the direction perpendicular to it, where the polarizing effect of Ca^{2+} sites reduces the diffusion of water molecules. On the other hand, solvent molecules can move preferentially along the 1-direction (characterized by anisotropic diffusion coefficient D_{11}) as a result of synergic interactions of the water molecules at the interface with the calcium, hydroxyl, and phosphate ions of the HAP surface.

Our study demonstrates and quantifies the anisotropic behaviour of fluid in bone nanostructures, which is an important area of bone biophysics (Lemaire et al. 2015a; Abdalrahman et al. 2015) and, therefore, gives new insights into the mechanisms controlling the motion of solvent molecules in confined spaces.

Acknowledgements The authors are grateful to the “Institut des sciences de l’ingénierie et des systèmes” (INSIS) of the “Centre national de la recherche scientifique” (CNRS) for financial support through the “HAP-W Nanopores” PEPS grant. The authors are also grateful to “Université Paris-Est Créteil” (UPEC) for the support of the French-English consortium. Finally, Dr. Muthuramalingam Prakash thanks UPEC for the funding of his post-doctoral research grant. This research utilised Queen Mary’s MidPlus computational facilities, supported by QMUL Research-IT, and funded by EPSRC Grant EP/K000128/1.

Compliance with ethical standards

Conflict of interest The authors declare that they have no conflict of interest.

References

Abdalrahman T, Scheiner S, Hellmich C (2015) Is trabecular bone permeability governed by molecular ordering-induced fluid viscosity gain? Arguments from re-evaluation of experimental

data in the framework of homogenization theory. *J Theor Biol* 365:433–444

Almora-Barrios N, Austen KF, de Leeuw NH (2009) Density functional theory study of the binding of glycine, proline, and hydroxyproline to the hydroxyapatite (0001) and (0110) surfaces. *Langmuir* 25(9):5018–5025

Berendsen H, Grigera J, Straatsma T (1987) The missing term in effective pair potentials. *J Phys Chem* 91(24):6269–6271 Berendsen HJ, Postma JP, van Gunsteren WF, Hermans J (1981)

Interaction models for water in relation to protein hydration. In: Pullman B (ed) *Intermolecular forces*. Springer, pp 331–342

Bhide SY, Berkowitz ML (2005) Structure and dynamics of water at the interface with phospholipid bilayers. *J Chem Phys* 123(22):224702

Boğan A, Rotenberg B, Marry V, Turq P, Noetinger B (2011) Hydrodynamics in clay nanopores. *J Phys Chem C* 115:16109–16115 Bolis V, Busco C, Martra G, Bertinetti L, Sakhno Y, Ugliengo P, Chiatti F, Corno M, Roveri N (2012) Coordination chemistry of Ca sites at the surface of nanosized hydroxyapatite: interaction with

H_2O and CO . *Philos Trans R Soc A* 370(1963):1313–1336

Bourg IC, Steefel CI (2012) Molecular dynamics simulations of water structure and diffusion in silica nanopores. *J Phys Chem C* 116(21):11556–11564

Chandra A (2000) Effects of ion atmosphere on hydrogen-bond dynamics in aqueous electrolyte solutions. *Phys Rev Lett* 85:768–771

Chandra A (2002) Structure and dynamics of hydrogen bonds in liquid water and aqueous solutions. *Proc Indian Natl Sci Acad* 69:49–69

Chiatti F, Corno M, Sakhno Y, Martra G, Ugliengo P (2013) Revealing hydroxyapatite nanoparticle surface structure by CO adsorption: a combined B3LYP and infrared study. *J Phys Chem C* 117(48):25526–25534

Cleveland G, Chang D, Hazlewood C, Rorschach H (1976) Nuclear magnetic resonance measurement of skeletal muscle: anisotropy of the diffusion coefficient of the intracellular water. *Biophys J* 16(9):1043–1053

Corno M, Rimola A, Bolis V, Ugliengo P (2010) Hydroxyapatite as a key biomaterial: quantum-mechanical simulation of its surfaces in interaction with biomolecules. *Phys Chem Chem Phys* 12(24):6309–6329

Cummings P, Wang B, Evans D, Fraser K (1991) Nonequilibrium molecular dynamics calculation of self-diffusion in a non-Newtonian fluid subject to a Couette strain field. *J Chem Phys* 94(3):2149–2158

Di Tommaso D, Ruiz-Agudo E, de Leeuw NH, Putnis A, Putnis CV (2014) Modelling the effects of salt solutions on the hydration of calcium ions. *Phys Chem Chem Phys* 16:7772–7785

- Essmann U, Perera L, Berkowitz ML, Darden T, Lee H, Pedersen LG (1995) A smooth particle mesh ewald method. *J Chem Phys* 103(19):8577–8593
- Fechete R, Demco D, Eliav U, Blümich B, Navon G (2005) Self-diffusion anisotropy of water in sheep achilles tendon. *NMR Biomed* 18(8):577–586
- Fernández-Seara MA, Wehrli SL, Wehrli FW (2002) Diffusion of exchangeable water in cortical bone studied by nuclear magnetic resonance. *Biophys J* 82(1):522–529
- Han KN, Bernardi S, Wang L, Searles DJ (2015) Water diffusion in zeolite membranes: molecular dynamics studies on effects of water loading and thermostat. *J Membr Sci* 495:322–333
- von Hansen Y, Gekle S, Netz RR (2013) Anomalous anisotropic diffusion dynamics of hydration water at lipid membranes. *Phys Rev Lett* 111(11):118103
- Hellmich C, Katti D (2015) Multiscale mechanics of biological, bioinspired, and biomedical materials. *MRS Bull* 40(04):309–313
- Hernandez SER, Streeter I, de Leeuw NH (2015) The effect of water on the binding of glycosaminoglycan saccharides to hydroxyapatite surfaces: a molecular dynamics study. *Phys Chem Chem Phys* 17(34):22377–22388
- Hille B (2001) Ion channels of excitable membranes, vol 507. Sinauer, Sunderland
- Holmboe M, Bourg IC (2014) Molecular dynamics simulations of water and sodium diffusion in smectite interlayer nanopores as a function of pore size and temperature. *J Phys Chem C* 118:1001–1013
- Holmes J, Davies D, Meath W, Beebe R (1964) Gas adsorption and surface structure of bone mineral. *Biochem* 3(12):2019–2024
- Holz M, Heil SR, Sacco A (2000) Temperature-dependent self-diffusion coefficients of water and six selected molecular liquids for calibration in accurate 1H NMR PFG measurements. *Phys Chem Chem Phys* 2:4740–4742
- Kandori K, Fudo A, Ishikawa T (2000a) Adsorption of myoglobin onto various synthetic hydroxyapatite particles. *Phys Chem Chem Phys* 2(9):2015–2020
- Kandori K, Mukai M, Yasukawa A, Ishikawa T (2000b) Competitive and cooperative adsorptions of bovine serum albumin and lysozyme to synthetic calcium hydroxyapatites. *Langmuir* 16(5):2301–2305
- Katti KS, Pradhan SM, Katti DR (2010) Mechanics of collagen in the human bone: role of collagen-hydroxyapatite interactions. In: *MRS Proceedings*, vol 1274. Cambridge Univ Press, pp 1274–QQ06–03
- Kirkpatrick R, Kalinichev A, Wang J (2005) Molecular dynamics modelling of hydrated mineral interlayers and surfaces: structure and dynamics. *Mineral Mag* 69(3):289–308. <http://www.ingentaconnect.com/content/minsoc/mag/2005/00000069/00000003/art00005>
- Kubicki J (ed) (2016) Molecular modeling of geochemical reactions: an introduction. Wiley, Chichester
- Kubo R (1957) Statistical-mechanical theory of irreversible processes. I. General theory and simple applications to magnetic and conduction problems. *J Phys Soc Jpn* 12(6):570–586
- de Leeuw NH (2004a) A computer modelling study of the uptake and segregation of fluoride ions at the hydrated hydroxyapatite (0001) surface: introducing a $\text{Ca}_{10}(\text{PO}_4)_6(\text{OH})_2$ potential model. *Phys Chem Chem Phys* 6(8):1860–1866
- de Leeuw NH (2004b) Resisting the onset of hydroxyapatite dissolution through the incorporation of fluoride. *J Phys Chem B* 108(6):1809–1811
- de Leeuw NH, Parker S (1998) Molecular-dynamics simulation of MgO surfaces in liquid water using a shell-model potential for water. *Phys Rev B* 58(20):13901
- Lemaire T, Pham T, Capiez-Lernout E, de Leeuw N, Naili S (2015a) Water in hydroxyapatite nanopores: possible implications for interstitial bone fluid flow. *J Biomech* 48(12):3066–3071
- Lemaire T, Pham TT, de Leeuw N, Naili S (2015b) Bone water at the nanoscale: a molecular dynamics study. *Comput Methods Biomech Biomed Eng* 18(sup1):1982–1983
- Liu P, Harder E, Berne B (2004) On the calculation of diffusion coefficients in confined fluids and interfaces with an application to the liquid–vapor interface of water. *J Phys Chem B* 108:6595–6602
- Lukasheva NV, Tolmachev DA (2015) Cellulose nanofibrils and mechanism of their mineralization in biomimetic synthesis of hydroxyapatite/native bacterial cellulose nanocomposites: molecular dynamics simulations. *Langmuir* 32(1):125–134
- Mkhonto D, de Leeuw NH (2002) A computer modelling study of the effect of water on the surface structure and morphology of fluorapatite: introducing a $\text{Ca}_{10}(\text{PO}_4)_6\text{F}_2$ potential model. *J Mater Chem* 12:2633–2642
- Nair AK, Gautieri A, Buehler MJ (2014) Role of intrafibrillar collagen mineralization in defining the compressive properties of nascent bone. *Biomacromolecules* 15(7):2494–2500
- Nguyen TX, Bhatia SK (2012) Some anomalies in the self-diffusion of water in disordered carbons. *J Phys Chem C* 116(5):3667–3676
- Nie GX, Wang Y, Huang JP (2016) Shape effect of nanochannels on water mobility. *Front Phys* 11(6):1–8
- Oddou C, Lemaire T, Pierre J, David B (2011) Hydrodynamics in porous media with applications to tissue engineering. In: Vafai K (ed) *Porous media: applications in biological systems and biotechnology*. CRC Press, Boca Raton, pp 75–119
- Parvaneh L, Donadio D, Sulpizi M (2016) Molecular mechanism of crystal growth inhibition at the calcium oxalate/water interfaces. *J Phys Chem C* 120(8):4410–4417
- Pham TT, Lemaire T, Capiez-Lernout E, Lewerenz M, To QD, Christie JK, Di Tommaso D, de Leeuw NH, Naili S (2015) Properties of water confined in hydroxyapatite nanopores as derived from molecular dynamics simulations. *Theor Chem Acc* 134(5):1–14
- Planchais A, Devautour-Vinot S, Salles F, Ragon F, Devic T, Serre C, Maurin G (2014) A joint experimental/computational exploration of the dynamics of confined water/zr-based mofs systems. *J Phys Chem C* 118(26):14441–14448
- Prakash M, Subramanian V (2011) Structure, stability and spectral signatures of monoprotic carborane acid–water clusters (CBW_n , where $n = 1–6$). *Phys Chem Chem Phys* 13(48):21479–21486
- Prakash M, Subramanian V, Gadre SR (2009) Stepwise hydration of protonated carbonic acid: a theoretical study. *J Phys Chem A* 113(44):12260–12275
- Prakash M, Jobic H, Ramsahye NA, Nouar F, Damasceno Borges D, Serre C, Maurin G (2015) Diffusion of H_2 , CO_2 , and their mixtures in the porous Zirconium based metal-organic framework MIL-140A(Zr): Combination of quasi-elastic neutron scattering measurements and molecular dynamics simulations. *J Phys Chem C* 119(42):23978–23989
- Qin Z, Gautieri A, Nair AK, Inbar H, Buehler MJ (2012) Thickness of hydroxyapatite nanocrystal controls mechanical properties of the collagen–hydroxyapatite interface. *Langmuir* 28(4):1982–1992
- Qiu T, Huang JP (2015) Unprecedentedly rapid transport of single-file rolling water molecules. *Front Phys* 10:1–8
- Rimola A, Corno M, Garza J, Ugliengo P (2012) Ab initio modelling of protein–biomaterial interactions: influence of amino acid polar side chains on adsorption at hydroxyapatite surfaces. *Philos T R Soc A* 370(1663):1478–1498
- Rohanizadeh R, Trécant-Viana M, Daculsi G (1999) Ultrastructural study of apatite precipitation in implanted calcium phosphate ceramic: influence of the implantation site. *Calcif Tissue Int* 64(5):430–436
- Sakhno Y, Bertinetti L, Iafisco M, Tampieri A, Roveri N, Martini G (2010) Surface hydration and cationic sites of

-
- nanohydroxyapatites with amorphous or crystalline surfaces: a comparative study. *J Phys Chem C* 114(39):16640–16648
- Salles F, Bourrelly S, Jobic H, Devic T, Guillermin V, Llewellyn P, Serre C, Ferey G, Maurin G (2011) Molecular insight into the adsorption and diffusion of water in the versatile hydrophilic/hydrophobic flexible MIL-53(Cr) MOF. *J Phys Chem C* 115(21):10764–10776
- Sansalone V, Naili S, Lemaire T (2012) Nanostructure and effective elastic properties of bone fibril. *Bioinspir Biomim Nanobiomater* 1(3):154–165
- Sansalone V, Kaiser J, Naili S, Lemaire T (2013) Interstitial fluid flow within bone canaliculi and electro-chemo-mechanical features of the canalicular milieu. *Biomech Model Mechanobiol* 12(3):533–553
- Sendner C, Horinek D, Bocquet L, Netz RR (2009) Interfacial water at hydrophobic and hydrophilic surfaces: slip, viscosity, and diffusion. *Langmuir* 25(18):10768–10781
- Srivastava R, Singh JK, Cummings PT (2012) Effect of electric field on water confined in graphite and mica pores. *J Phys Chem C* 116(33):17594–17603
- Su J, Guo H (2011) Effect of nanotube-length on the transport properties of single-file water molecules: transition from bidirectional to unidirectional. *J Chem Phys* 134(24):244513
- Sudarsanan KT, Young R (1969) Significant precision in crystal structural details. Holly Springs hydroxyapatite. *Acta Crystallogr Sect B* 25(8):1534–1543
- Tan HS, Piletic IR, Fayer M (2005) Orientational dynamics of water confined on a nanometer length scale in reverse micelles. *J Chem Phys* 122(17):174501
- Thomsen C, Henriksen O, Ring P (1987) In vivo measurement of water self diffusion in the human brain by magnetic resonance imaging. *Acta Radiol* 28(3):353–361
- Tian KV, Mahmoud MZ, Cozza P, Licoccia S, Fang D-C, Di Tommaso D, Chass G, Greaves GN (2016) Periodic vs. molecular cluster approaches to resolving glass structure and properties: Anorthite a case study. *J Non-Cryst Solids* 451:138–145
- Todorov IT, Smith W, Trachenko K, Dove MT (2006) DL-POLY 3: new dimensions in molecular dynamics simulations via massive parallelism. *J Mater Chem* 16(20):1911–1918
- Wei MJ, Zhou J, Lu X, Zhu Y, Liu W, Lu L, Zhang L (2011) Diffusion of water molecules confined in slits of rutile TiO₂ (110) and graphite (0001). *Fluid Phase Equilib* 302(1):316–320
- Weiner S, Traub W (1986) Organization of hydroxyapatite crystals within collagen fibrils. *FEBS Lett* 206:262–266
- Wierzbicki A, Cheung HS (2000) Molecular modeling of inhibition of hydroxyapatite by phosphocitrate. *J Mol Struct (THEOCHEM)* 73(1–3):73–82
- Xu L, Hu YZ, Ma TB, Wang H (2013) Tunable giant anisotropic diffusion of water sub-monolayers between graphene layers. *Nanotechnology* 24(50):505504
- Yoon YJ, Cowin SC (2008) The estimated elastic constants for a single bone osteonal lamella. *Biomech Model Mechanobiol* 7(1):1–11
- Young T (2016) Atten. coordinate creator and editor for atomistic simulations, including periodic systems. <https://www.projectaten.com>
- Zhao W, Xu Z, Yang Y, Sahai N (2014) Surface energetics of the hydroxyapatite nanocrystal–water interface: a molecular dynamics study. *Langmuir* 30(44):13283–13292